PAPER

Layer- and substrate-dependent charge density wave criticality in 1T–$TiSe_2$

To cite this article: Sadhu Kolekar *et al* 2018 *2D Mater.* **5** 015006

View the article online for updates and enhancements.

Related content

- Substrate dependent electronic structure variations of van der Waals heterostructures of MoSe2 or MoSe2(1x)Te2x grown by van der Waals epitaxy
Horacio Coy Diaz, Yujing Ma, Sadhu Kolekar et al.
- An alternative interpretation of recent ARPES measurements on TiSe2
J. van Wezel, P. Nahai-Williamson and S. S. Saxena
- Suppression and emergence of charge-density waves at the surfaces of layered 1T-TiSe2 and 1T-TaS2 by in situ Rb deposition
K Rossnagel

Recent citations

- Charge Order of Strongly Bounded Electron Pairs on the Triangular Lattice: the Zero-Bandwidth Limit of the Extended Hubbard Model with Strong Onsite Attraction
Konrad Jerzy Kapcia
- Controlling the Charge Density Wave Transition in Monolayer TiSe2 : Substrate and Doping Effects
Sadhu Kolekar *et al*
- Pseudogap, Fermi arc, and Peierls-insulating phase induced by 3D–2D crossover in monolayer VSe2
Yuki Umemoto *et al*

IOP ebooks™

Bringing you innovative digital publishing with leading voices to create your essential collection of books in STEM research.

Start exploring the collection - download the first chapter of every title for free.

This content was downloaded from IP address 131.247.208.45 on 03/04/2019 at 21:51

2D Materials

PAPER

RECEIVED
17 July 2017

REVISED
15 September 2017

ACCEPTED FOR PUBLICATION
22 September 2017

PUBLISHED
5 October 2017

Layer- and substrate-dependent charge density wave criticality in 1T–$TiSe_2$

Sadhu Kolekar, Manuel Bonilla, Yujing Ma, Horacio Coy Diaz and Matthias Batzill

Department of Physics, University of South Florida, Tampa, FL 33620, United States of America

E-mail: mbatzill@usf.edu

Keywords: $TiSe_2$, exciton condensate, monolayer, scanning tunneling spectroscopy, exciton insulator

Abstract

$TiSe_2$ exhibits an unconventional charge density wave (CDW) that has been associated with an excitonic insulator transition. Here we investigate how the CDW transition is changed for single to few layers compared to bulk $TiSe_2$. $TiSe_2$ grown by molecular beam epitaxy on HOPG- or MoS_2-substrates is characterized by variable temperature scanning tunneling microscopy and spectroscopy. We show that the CDW state persists for the monolayer but the transition temperature T_{CDW} is significantly increased compared to the bulk. Furthermore, T_{CDW} is strongly dependent on the substrate material. Within the model of an excitonic insulator phase for $TiSe_2$, the substrate dependence may be associated with variations of the excitonic binding energies by the dielectric properties of the substrate. Interestingly, for single layer $TiSe_2$ on HOPG we also observe peaks in the tunneling spectra below 50 K, which are tentatively assigned to coherence peaks of an excitonic condensate. The peaks are observed below T_{CDW} of ~230 K, suggesting that an excitonic insulator induced CDW can exist without a phase coherent state.

It has been demonstrated that reducing the dimensions to a single-layer enables modifications of conventional charge density waves (CDW) in metallic transition metal dichalcogenides (TMDCs) [1, 2]. For $TiSe_2$, however, traditional explanations for CDW formation, based on Fermi surface nesting, fail [3]. Instead, an unconventional excitonic mechanism has been invoked [4, 5]. This implies a CDW dependence on the number of layers because the exciton binding energy is increased in single layer TMDCs compared to bulk [6].

Bulk $TiSe_2$ forms a commensurate $2 \times 2 \times 2$ CDW with a transition temperature around 200 K. In view of Fermi wave-vector nesting failing to explain CDW in $TiSe_2$, the CDW transition has been proposed to be related to a Jahn–Teller like lattice distortion [7, 8], the formation of an excitonic condensate [9–12], or a combination of these effects [13]. The interest in $TiSe_2$ has also been fueled by recent discoveries that showed that superconductivity can be induced by copper doping [14] or field-effect doping of few-layer $TiSe_2$ [15]. In both cases the suppression of the CDW [16] is considered essential in order to achieve superconductivity.

The basic electronic structure of $TiSe_2$ consists of strongly dispersing Se-4p derived valence bands (three bands have been identified in ARPES) at the Γ-point and Ti-3d derived electron-pockets at the *M*-points of the Brillouin zone (BZ) boundary. There is increasing evidence that the Se-4p and Ti-3d states do not overlap even in the normal state and instead exhibit an energy gap of ~50 meV. Upon formation of $2 \times 2(\times 2)$ CDW, strong 'umklapp' shadow bands are formed. The electronic structure in the normal- and the 2×2 CDW-phase are schematically shown in figure 1. Recent ARPES studies on single-layer samples indicate a similar valence band structure to bulk samples, with some increase in the binding energy of the valence band maximum [17, 18]. Generally, ARPES also agrees for both single layer as well as bulk samples that the bottom of the Ti-3d band is occupied at the *M*-point. However, while the Se-4p band shows strong spectral weight at the *M*-point in the CDW phase, no intensity of the Ti-3d states at the Γ-point are observed in ARPES [12, 17,18]. The vanishing spectral weight of such a Ti-3d umklapp-band at Γ has been explained in the picture of an excitonic insulator [9]. In this model, the Fermi-level should lie close-to mid-gap for the band gap of the excitonic insulator phase at Γ, as illustrated in figure 1.

The band structure of $TiSe_2$ makes it potentially susceptible to formation of an excitonic condensate as the basic mechanism for formation of the CDW. This mechanism was first predicted in the 1960s and

© 2017 IOP Publishing Ltd

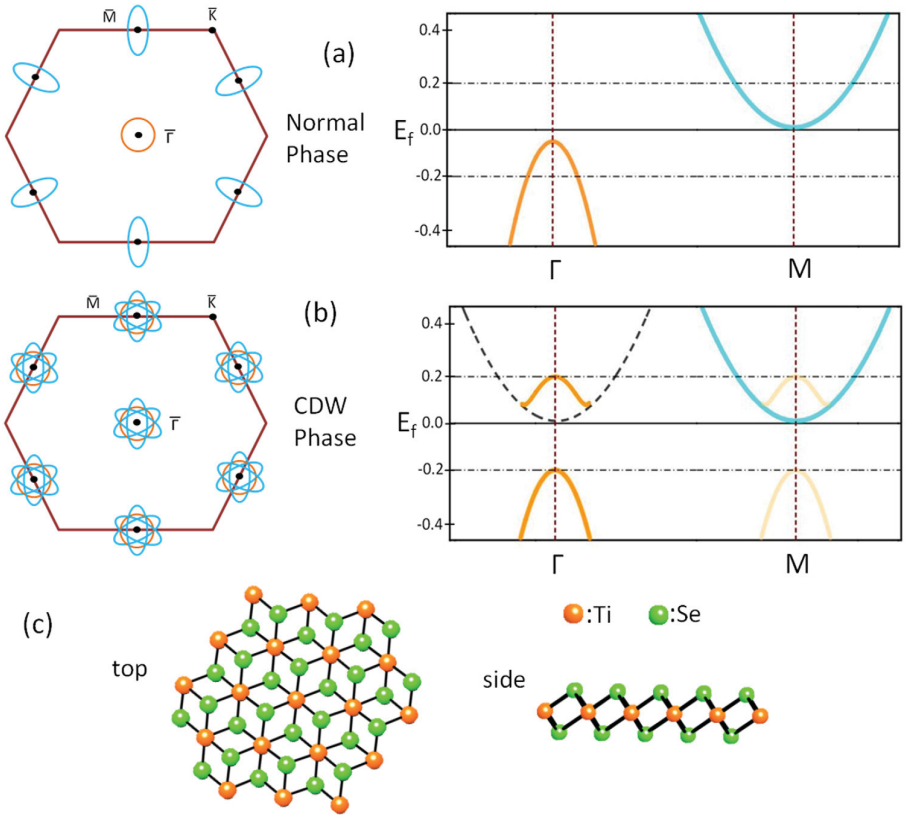

Figure 1. Electronic and structural characteristics of $TiSe_2$. Schematic of electronic structure of $TiSe_2$ in its normal phase is shown in (a). At the Γ-point the Se-4p band forms a hole pocket, while at the *M*-point the Ti-3d band forms an electron-pocket indicated by orange and blue lines, respectively. ARPES measurements have indicated that the Fermi-level lies close to the bottom of the Ti-3d band. The electronic-structure in the CDW-phase is shown in (b). Umklapp replica bands for the 2×2 structure are expected at Γ and *M*, as well as an opening of a gap. The down-ward shift of the Se-4p band has been previously detected in ARPES. In the excitonic insulator model the spectral weight of the umklapp band is shifted away from the Fermi-level (see [9] for details) forming a band gap at the Γ-point with the Fermi-level lying close to the midgap position. A ball-and-stick model of the 1T structure of $TiSe_2$ single layer is illustrated in (c).

may be expected for a material with the valence band and conduction band offset in k-space with either a small energy overlap or gap [19, 20]. In such a material spontaneous excitation of electrons from the valence band into the conduction band could become energetically favorable if the electron–hole pair (exciton) binding energy is larger than the energy cost for promoting electrons to the conduction band, i.e. the band gap energy. In this scenario, the exciton binding energy is related to the order parameter in a BCS like description of the CDW phase transition, implying that the transition temperature should be related to the exciton binding energy. Generally, the exciton binding energy is a material property and cannot be easily modified. For TMDCs, however, the exciton binding energy has been demonstrated to increase markedly with the decrease of number of layers. Consequently, if the excitonic insulator model for the CDW in $TiSe_2$ is valid, the increased exciton binding energy for monolayers is expected to result in a larger CDW-gap and an increased transition temperature for monolayers compared to bulk $TiSe_2$ may be predicted. Moreover, the excitonic binding energy for a monolayer is tuned by the dielectric properties of the material surrounding the monolayer [21, 22]. Consequently, the CDW transition may depend on dielectric properties of the substrate material the $TiSe_2$ monolayer is supported on.

Here we investigate the properties of $TiSe_2$ with variable temperature scanning tunneling spectroscopy (STS). STS enables measuring the opening of a gap between valence and conduction band and thus makes it a valuable tool for characterizing many body phenomena [23]. However, STS does not provide momentum resolved information and STS mainly probes states around Γ-point, specifically for 2D materials. We observe a band gap opening that is significantly larger for the single layer than the few layer materials. Moreover, the band gap strongly depends on the substrate material. Using variable temperature STS we can determine the transition temperature by fitting of the band gap to a mean field theory expression. Interestingly, we also observe pronounced peaks close to the band edges in the differential conductance for $TiSe_2$/HOPG at below 50 K. We tentatively assign these pronounced peaks to phase coherence peaks expected to exist in an isotropic Bose–Einstein condensate of excitons.

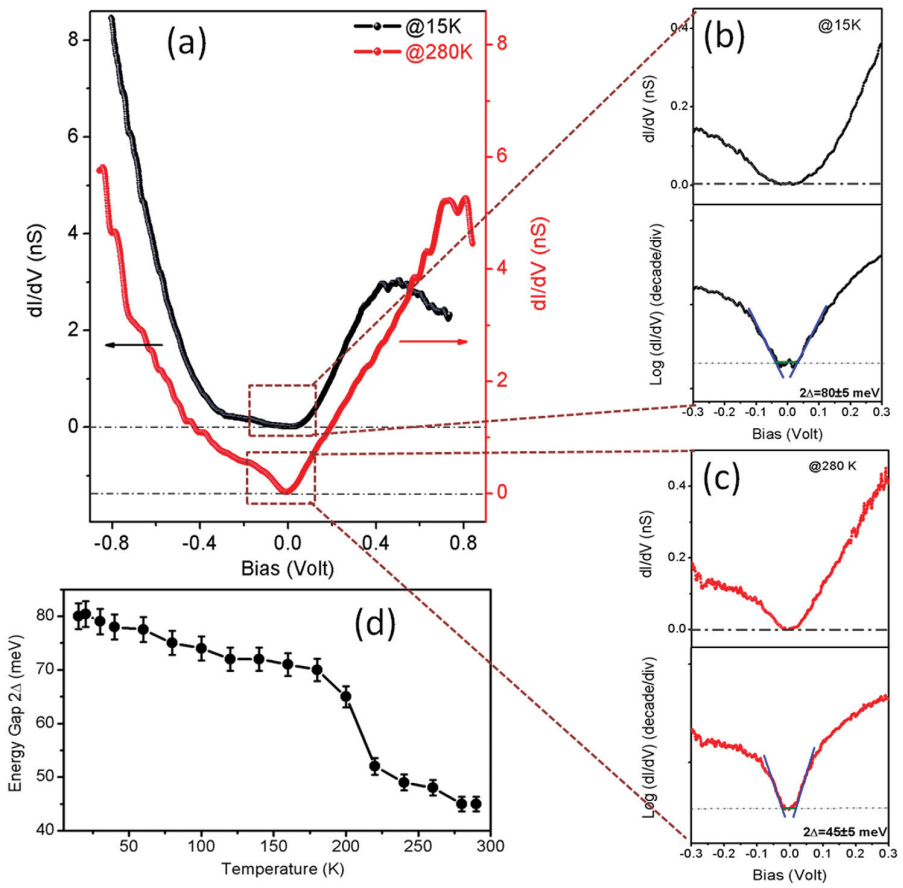

Figure 2. Temperature dependent scanning tunneling spectroscopy on a bulk $TiSe_2$ single crystal surface. The differential conductance at 15 K and 280 K is shown in (a) and the respective detailed measurements of the band gap are shown in (b) and (c) on a linear and logarithmic scale. The band gaps are determined in the logarithmic plots. A transition of the CDW gap of ~80 meV to the normal gap of ~45 eV occurs at 200 K as shown in (d).

Results

Before addressing monolayer samples, we discuss measurements on bulk $TiSe_2$ to provide a comparison to the few and monolayer samples. Figure 2 shows STS measurements on a single crystal $TiSe_2$ sample with our spectra being consistent with previously reported data on bulk samples [24]. We are extracting the band gap as a function of temperature by plotting differential conductance dI/dV and finding the valence band maximum and conduction band minimum by extrapolating the respective band edges to zero. With this approach, we find a small gap of ~45 meV for the normal state at RT and a slightly larger gap of ~80 meV at 15 K. The dependence of the measured gap on temperature is displayed in figure 2(d). A transition from the lower to the larger band gap value occurs at ~200 K, consistent with the reported CDW transition of $TiSe_2$. These measurements give a value for $2\Delta/(k_B\ T_c) = 80\ \text{meV}/(k_B\ 200\,\text{K}) = 4.64$, i.e. a slightly larger value than the prediction of conventional BCS theory of 3.65. The larger value is explained by stronger quasiparticle coupling.

$TiSe_2$ thin films grown by MBE enable the investigation of the dependence of the CDW band gap as a function of the number of $TiSe_2$ layers. Figure 3 shows room temperature STM images of typical $TiSe_2$ films. The large-scale image shows the formation of extended monolayer terraces with some bilayer islands. Atomic scale images of the terraces show good quality similar to previously reported MBE-grown $TiSe_2$ [25]. For further spectroscopic characterization the MBE grown samples were transferred in a vacuum suitcase to a dedicated variable temperature STM. In order to characterize the dependence of the electronic structure on the number of layers we choose a sample-region that exhibits non-uniform film thickness, possibly at a growth spiral. The band gap measurement at 15 K, i.e. in CDW phase, is shown in figure 4 as a function of layers determined from the step height separating the individual terraces. For only 3 layers the band gap measurement is, to within the experimental uncertainty, the same as the band gap of bulk surfaces. For one- and two-layer thick samples the band gap is significantly larger and we measure ~180 meV for the monolayer film. Moreover, the differential conductance for the monolayer exhibits prominent peaks that are not present in bulk $TiSe_2$. For the monolayer $TiSe_2$, thesepeaks appear at energies below the valence band maximum and above the conduction band minimum.

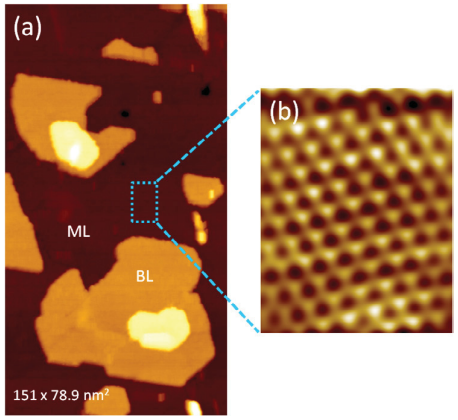

Figure 3. STM images of MBE grown $TiSe_2$. (a) Large scale RT scanning tunneling microscopy image indicating monolayer (ML) and bilayer (BL) regions. (b) Atomic resolution image of the monolayer showing a 1 × 1 structure at RT.

Comparison with two independent ARPES measurements for monolayer $TiSe_2$ [17,18], shows that the energy of the peaks corresponds closely to the band maximum of the Se-4p band. All the measurements have been reproduced on three independent samples and at several spots on these samples.

In order to demonstrate that these peaks are associated with a 2 × 2 charge density wave in the monolayer, we performed dI/dV mapping with set-points below (120 mV) and at (200 mV) the peak position. Figures 4(d) and (e) shows the dI/dV maps. For 120 mV set-point only weak modulations are observed while at 200 mV a clear 2 × 2 intensity modulation is observed corresponding to the CDW periodicity. This illustrates that even for the monolayer a 2 × 2 charge modulation is observed and the pronounced peaks in the differential conductance measurement are related to this CDW modulation.

In further investigations, we characterize the band gap measured in STS as a function of sample temperature, as shown in figure 5(a). The first observation is that the pronounced peaks become strongly suppressed and vanish completely at ~50 K (figures 5(c) and (d)), while the STS-band gap remains unaltered. The disappearance of the peaks in differential conductance indicates that they are associated with a thermally driven transition. The fact that this transition is below T_{CDW} shows that the CDW can form independent of the observation of the pronounced peaks in differential conductance. Further increase in sample temperature leads eventually to a reduced band gap and the band gap reaches the same value as for the normal phase in bulk $TiSe_2$. This demonstrates that the band gap opening is entirely a consequence of the CDW transition. As expected an increased band gap for single layer also translates into an increase in T_{CDW} from ~200 K to ~230 K. A similar increase in T_{CDW} for monolayer $TiSe_2$ on graphene has recently been deduced from photoemission measurements [18].

A possible explanation for the strongly increased CDW-gap in single-layer materials is the increased exciton binding energy in single-layer TMDCs compared to bulk materials leading to a larger magnitude of the order parameter in an excitonic insulator driven CDW transition [9]. A test for the correlation between CDW in $TiSe_2$ and the excitonic binding energy is to vary the excitonic binding energy. Ordinarily the excitonic binding energy of a material is a material property. However, in monolayers TMDCs the surrounding dielectric material influences the Coulomb screening of electron–hole pairs. Replacing the HOPG substrate with a wide band gap semiconducting van der Waals material is expected to reduce charge screening and thus increase the exciton binding energy. Here we choose MoS_2 as such a material. Figure 5(b) shows STS spectra for monolayer $TiSe_2$ on MoS_2 as a function of temperature. In agreement with the excitonic picture, the band gap in the CDW phase and T_c is significantly increased for $TiSe_2/MoS_2$ system compared to $TiSe_2$ on HOPG. Interestingly, contrary to $TiSe_2$/HOPG no pronounced peaks in the differential conductance are observed down to lowest accessible temperature of 15 K.

Discussion

The variation of the STS band gaps for bulk $TiSe_2$ as well as for single layer $TiSe_2$ on HOPG and MoS_2 substrates follow an expected mean field theory temperature dependence as shown in figure 6. The data are fit based on the mean-field theory expression [18]:

$$\Delta^2(T) - \Delta^2(T_{CDW}) \sim \tanh^2\left(A\sqrt{\frac{TCDW}{T} - 1}\right), \quad (1)$$

where $A = 2.1$ is a proportionality constant, and $\Delta(T)$ and $\Delta(T_{CDW})$ is the energy gap at temperature T, and the constant value for the energy gap above the critical temperature T_{CDW}, respectively. The Transition temperature derived from this fitting agrees with the generally accepted T_c for bulk $TiSe_2$ of ~200 K and shows an increase to 230 K and 280 K for monolayers on HOPG and MoS_2, respectively. This increase in CDW transition temperature for monolayer $TiSe_2$ from HOPG to MoS_2 substrate is consistent with the measured large energy gaps. A larger exciton binding energy for single layer $TiSe_2$ supported on the semi-conducting MoS_2 compared to the semi-metallic graphite is expected. Consequently, the trend of an increased T_{CDW} for monolayer $TiSe_2$ on MoS_2 compared to HOPG, is also consistent within the model of an excitonic insulator phase which suggests a scaling of the transition temperature with the excitonic binding energy.

It is important to compare our STS work with previously reported ARPES studies both on bulk [5, 9, 12] and monolayer $TiSe_2$ samples [17, 18]. In ARPES measurements an opening of a gap below the Fermi-level is observed with the Ti-3d state at the Fermi-level remaining at the M-point. Only a down ward shift of

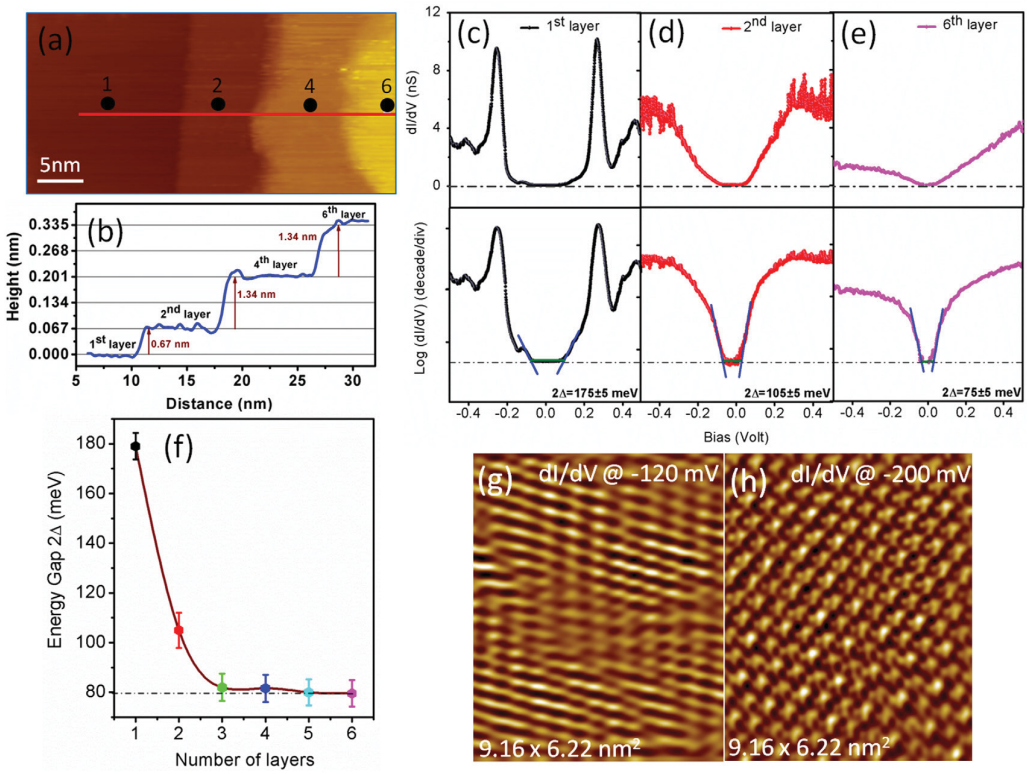

Figure 4. CDW gap as a function of number of layers for a $TiSe_2$ film on HOPG measured at 15 K. Terraces with different number of layers are shown in (a) and the corresponding line scan in (b). Characteristic differential conductance measurements and their corresponding logarithmic plots for a single layer, bi-layer, and 6 layers are shown in (c)–(e) respectively. The CDW-band gaps extracted from the logarithmic differential conductance plots are plotted as a function of number of layers in (f). For only 3-layer thick films a CDW gap similar to that of bulk samples is obtained. For the single layer the differential conductance spectrum, shown in inset (c) exhibits pronounced coherence peaks. (g) and (h) Show dI/dV maps for single layer $TiSe_2$ at bias set-points of −120 mV, −200 mV, respectively. These set-points are also indicated in (c) by the red points and correspond to below and at the coherence peak position. The dI/dV map at the coherence point exhibit strong modulations with a 2 × 2 periodicity, suggesting that the coherence peaks are associated with the CDW.

the Se-4p states is observed in ARPES for temperatures below the CDW transition. We may compare the ARPES Se-4p band maximum as a function of temperature for monolayer $TiSe_2$ on grapheme [17, 18] with our STS data. It is apparent that the pronounced peak in the differential conductance at low temperature coincides with the Se-4p band maximum in ARPES data and thus this feature should be assigned to the band maximum of Se-4p. However, no further states are observed in ARPES between the Se-4p band maximum and the Ti-3d conduction band and thus we currently cannot explain the small intensity observed in STS above the Se-4p state. Nevertheless, we use this onset for plotting the band gap versus temperature because it is the only reliable feature at elevated temperatures or for enabling comparison with $TiSe_2$ on MoS_2 substrates.

While ARPES cannot measure the conduction band, a partially occupied Ti-3d band at the M-point is consistently observed in ARPES indicating that the Fermi-level lies very close to the bottom of the Ti-3d band. On the other hand, while the umklapp Se-4p band is observed in ARPES at the 'original' M-point of the BZ, no indication of an equivalent umklapp Ti-3d band at the Γ-point is observed in ARPES studies [17]. Such a negligible spectral weight of an umklapp Ti-3d state has been explained theoretically for an excitonic insulator phase [9]. Thus our STS data can be reconciled with the ARPES data, because in STS we are most sensitive to states at the Γ-point. This is in particularly true for 2D materials. In general, it is established that the tunneling current is dominated by states with a large velocity component normal to the surface and consequently states with in-plane momenta are contributing less to the tunneling signal, which has been referred to the 'tunneling cone' [26]. Thus we propose that the observed STS-gap reflects only the magnitude of the gap at the Γ-point, while the metallic Ti-3d states at the M-point are of negligible intensity in our STS data. Furthermore, we also expect the Fermi-level to lie close to mid-gap in the excitonic insulator phase at the Γ-point, as sketched in figure 1. Moreover, the excitonic condensate state has been predicted at ~150 meV above the Fermi-level for an order parameter of 100 meV [9] similar to the observed position of the peak in differential conductance.

The strong and reproducible peaks in the differential conductance for single layer $TiSe_2$ on HOPG and their well-defined temperature dependence require some explanation. Their appearance is similar to

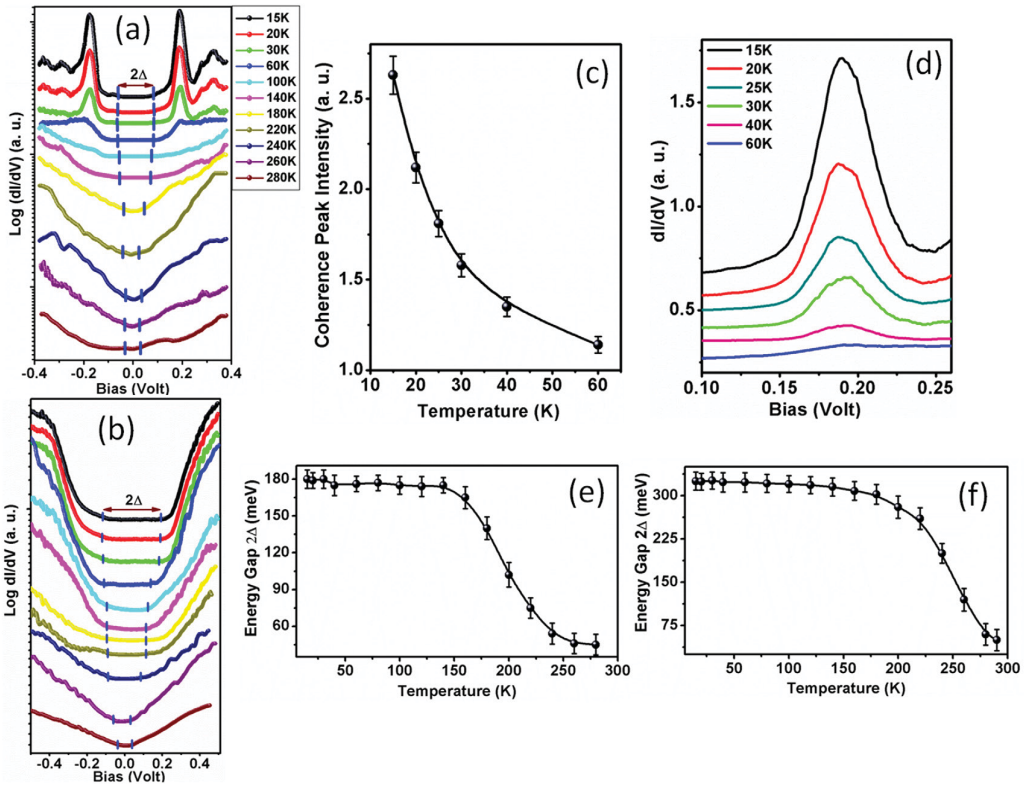

Figure 5. Temperature dependent differential conductance spectra for single layer $TiSe_2$ on HOPG- and MoS_2-substrates. The differential conductance of $TiSe_2$ on HOPG is shown in (a) and for $TiSe_2$ on MoS_2 in (b). The change of the coherence peak as a function of T is shown in (c) and (d). The band edges are marked in (a) and (b) by short lines and the band gap is plotted in (e) for $TiSe_2$ on HOPG and in (f) for $TiSe_2$ on MoS_2.

coherence peaks in superconductors below T_c, albeit the larger energy gap observed for the CDW in $TiSe_2$. If an excitonic condensate is formed the excitons are expected to also form a phase coherent state and this should be observed in STS as coherence peaks. To the best of our knowledge, no such peaks have ever been reported for $TiSe_2$, nor do we observe it for any other material than single layer $TiSe_2$ on HOPG. Moreover, it is only observed below 50 K, i.e. significantly below T_{CDW}. Thus, the absence of these peaks in certain materials would suggest that an excitonic insulator phase may form without long range phase coherence.

The lack of coherence-peaks for monolayer-$TiSe_2$/MoS_2 also suggests that phase coherence can be easily destroyed by, for example, stronger scattering mechanisms in such heterostructures compared to $TiSe_2$/HOPG samples. Scattering may be related to a stronger interlayer coupling because of interlayer hybridization of frontier orbitals in TMDC heterostructures [27]. Electronic interlayer coupling give rise to stronger scattering or even interlayer excitons as observed in semiconducting van der Waals TMDC-heterostructures [28, 29]. Thus, we predict that the coherent state may only be observed in weakly coupled heterostructures, such as observed for $TiSe_2$/HOPG, or truly freestanding single layer $TiSe_2$. Clearly, further studies are required to verify the assignment of the pronounced peaks in STS to coherence peaks. For a start, contactless measurements for $TiSe_2$/HOPG by for example ARPES would be important.

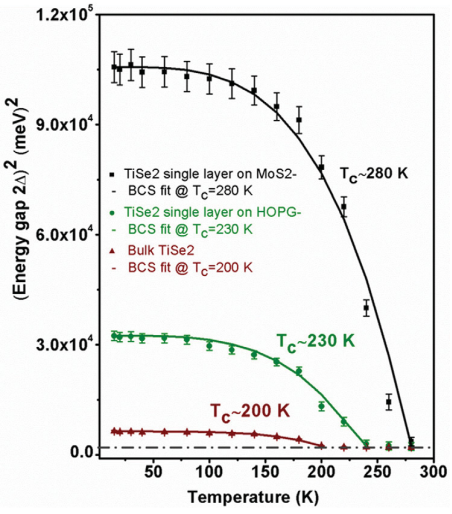

Figure 6. Mean field theory fitting of the band gap versus temperature for CDW transitions. Data for $TiSe_2$ single layer on HOPG- and MoS_2-substrates as well as for bulk $TiSe_2$ are shown. The mean-field theory is best fit with transition temperatures of 200 K, 230 K, and 280 K for bulk $TiSe_2$, single layer on HOPG, and single layer on MoS_2, respectively.

Conclusions

In conclusion, the CDW transition temperature in single layer is increased compared to bulk $TiSe_2$ and can be further controlled by the choice of support. The increase in the gap can be understood by variations in the excitonic binding energy in TMDCs and thus is consistent with an excitonic origin for the CDW in $TiSe_2$. Interestingly, pronounced peaks in the differential conductance for $TiSe_2$ monolayers on HOPG are observed which we tentatively attribute to the formation of a phase coherent state in an excitonic condensate. In general, this study shows that new insight in many body physics of layered TMDCs can be gleaned from studying monolayers and their interfaces. Moreover, we demonstrated the potential for tuning many body physics in these materials by growing van der Waals heterostructures.

Methods

Mono- to few-layer $TiSe_2$ was grown on HOPG or MoS_2 substrates by e-beam evaporation of Ti and simultaneous deposition of atomic Se from a hot wall Se-cracker source. The substrates were cleaved in air and immediately introduced into the vacuum chamber. The substrates were subsequently annealed in UHV at 300 °C for 5 h prior to film growth. $TiSe_2$ was grown at a substrate temperature of 200 C and at a growth rate of 0.56 ml min^{-1}. After growth, the samples were characterized by XPS and room temperature STM before transferring them in a vacuum suitcase to a variable temperature STM. This STM is a commercial Pan-style RHK STM. A closed cycle cryostat allowed cooling of the sample to a minimum of 15 K and the sample could be heated in the cryostat to various target temperatures. STM and STS was taken with a cut PtIr-tip. For dI/dV spectroscopy a lock-in amplifier with a modulation voltage of 7 mV and reference frequency 995 Hz was used. For reference, we also conducted spectra on bulk $TiSe_2$ single crystals. STS measurements on $TiSe_2$ single crystals were previously published and our data are in good agreement with such studies confirming consistency of our data with those in different groups.

Acknowledgement

The authors acknowledge support from the National Science Foundation under grant DMR-1701390.

Notes

The authors declare no competing financial interests.

ORCID iDs

Matthias Batzill https://orcid.org/0000-0001-8984-8427

References

[1] Xi X, Zhao L, Wang Z, Berger H, Forró L, Shan J and Mak K F 2015 Strongly enhanced charge-density-wave order in monolayer $NbSe_2$ *Nat. Nanotechnol.* **10** 765–70
[2] Ugeda M M *et al* 2016 Characterization of collective ground states in single-layer $NbSe_2$ *Nat. Phys.* **12** 92–8
[3] Rossnagel K 2011 On the origin in charge-density waves in selected layered transition-metal dichalcogenides *J. Phys.: Condens. Matter* **23** 213001
[4] Cercellier H *et al* 2007 Evidence for an excitonic insulator phase in 1T–$TiSe_2$ *Phys. Rev. Lett.* **99** 146403
[5] Monney C, Battaglia C, Cercellier H, Aebi P and Beck H 2011 Exciton condensation driving the periodic lattice distortion of 1T–TiSe2 *Phys. Rev. Lett.* **106** 106404
[6] Olsen T, Latini S, Rasmussen F and Thygesen S K 2016 Simple screened hydrogen model of excitons in two-dimensional materials *Phys. Rev. Lett.* **116** 056401
[7] Zunger A and Freeman A J 1978 Band structure and lattice instability of $TiSe_2$ *Phys. Rev.* B **17** 1839–42
[8] Suzuki N, Yamamoto A and Motizuki K 1985 Microscopic theory OF the CDW state of 1T–TiSe2 *J. Phys. Soc. Japan* **54** 4668–79
[9] Monney C *et al* 2009 Spontaneous exciton condensation in 1T–$TiSe_2$: BCS-like approach *Phys. Rev.* B **79** 045116
[10] Möhr-Vorobeva E, Johnson S L, Beaud P, Staub U, De Souza R, Milne C, Ingold G, Demsar J, Schaefer H and Titov A 2011 Nonthermal melting of a charge density wave in $TiSe_2$ *Phys. Rev. Lett.* **107** 036403
[11] May M M, Brabetz C, Janowitz C and Manzke R 2011 Charge-density-wave phase of 1T–$TiSe_2$: the influence of conduction band population *Phys. Rev. Lett.* **107** 176405
[12] Rohwer T *et al* 2011 Collapse of long-range order tracked by time-resolved photoemission at high momenta *Nature* **471** 490–3
[13] Van Wezel J, Nahai-Williamson P and Saxena S S 2010 An alternative interpretation of recent ARPES measurements on $TiSe_2$ *Euro. Phys. Lett.* **89** 47004
[14] Morisan E 2006 Superconductivity in Cu_xTiSe_2 *Nat. Phys.* **2** 544–50
[15] Li L J, O'Farrell E C T, Loh K P, Eda G, Özyilmaz B and Castro Neto A H 2016 Controlling many-body states by the electric-field effect in a two-dimensional material *Nature* **529** 185–9
[16] Joe Y I *et al* 2014 Emergence of charge density wave domain walls above the superconducting dome in 1T–$TiSe_2$ *Nat. Phys.* **10** 421–5
[17] Sugawara K, Nakata Y, Shimizu R, Han P, Hitosugi T, Sato T and Takahashi T 2016 Unconventional charge-density-wave transition in monolayer 1T–$TiSe_2$ *ACS Nano* **10** 1341–5
[18] Chen P, Chan Y H, Fang X-Y, Zhang Y, Chou M Y, Mo S-K, Hussain Z, Fedorov A-V and Chiang T C 2015 Charge density wave transition in single-layer titanium diselenide *Nat. Commun.* **6** 8943
[19] Keldysh L V and Kopaev Y V 1965 Possible instability of the semimetallic state toward Coulomb interactiosn *Sov. Phys. Solid State* **6** 2219–24
[20] Jérome D, Rice T M and Kohn W 1967 Excitonic insulator *Phys. Rev.* **158** 462–75
[21] Ugeda M M *et al* 2014 Giant bandgap renormalization and excitonic effects in a monolayer transition metal dichalcogenide semiconductor *Nat. Mater.* **13** 1091–5
[22] Stier A V, Wilson N P, Clark G, Xu X and Crooker S A 2016 Probing the influence of dielectric environment on excitons in monolayer WSe_2: insight from high magnetic fields *Nano Lett.* **16** 7054–60
[23] Fischer Ø, Kugler M, Maggio-Aprile I, Berthod C and Renner C 2007 Scanning tunneling spectroscopy of high-temperature superconductors *Rev. Mod. Phys.* **79** 353–419
[24] Hildebrand B, Didiot C, Novello A M, Monney G, Scarfato A, Ubaldini A, Berger H, Bowler D R, Renner C and Aebi P 2014 Doping nature of native defects in 1T–$TiSe_2$ *Phys. Rev. Lett.* **112** 197001
[25] Peng J-P, Guan J-Q, Zhang H-M, Song C-L, Wang L, He K, Xue Q-K and Ma X-C 2015 Molecular beam epitaxy growth

and scanning tunneling microscopy study of $TiSe_2$ ultrathin films *Phys. Rev.* B **91** 121113
[26] Beuermann G 1981 On the directional selectivity of tunneling experiments *Z. Phys.* B **44** 29–31
[27] Wilson N R *et al* 2017 Determination of band offsets, hybridization, and exciton binding in 2D semiconductor heterostructures *Sci. Adv.* **3** e1601832
[28] Rivera P *et al* 2015 Observation of long-lived interlayer excitons in monolayer MoSe2–WSe_2 heterostructures *Nat. Commun.* **6** 6242
[29] Yu Y *et al* 2015 Equally efficient interlayer exciton relaxation and improved absorption in epitaxial and nonepitaxial MoS_2/WS_2 heterostructures *Nano Lett.* **15** 486–91